Invited Paper

Space-based planet detection using two MEMS DMs and a shaped pupil

N. Jeremy Kasdin[a], T. Groff[a], A. Carlotti[a], R. Vanderbei[a]

[a]Princeton University, Princeton, NJ, 08544 USA

ABSTRACT

NASA and the astronomy community hope to soon launch a new space-based telescope to detect and characterize extrasolar planets. Detecting extrasolar planets with angular separations and contrast levels similar to Earth requires not only a large space-based observatory but also advanced starlight suppression techniques. One promising approach is coronagraphy via shaped pupils. Shaped pupil coronagraphs are binary pupil functions that modify the point spread function of a telescope to produce regions of high contrast. Unfortunately, the contrast performance of coronagraphs is highly sensitive to optical errors, thus necessitating wavefront control to retrieve the necessary contrast levels. Using two MEMS deformable mirrors in series with the coronagraph allows us to control both the phase and amplitude aberrations over a finite wavelength range. Given an estimate of the wavefront we have developed an optimal controller that minimizes actuator strokes on the deformable mirrors subject to a constraint that it achieve a targeted contrast level in a defined region of the image. To provide an estimate for the controller that is accurate enough to converge to a solution that achieves the required ten orders of magnitude, the electric field must be estimated using the science camera to avoid any non-common path errors. The estimate is found by either using a batch process or Kalman filter technique which uses multiple image pairs with conjugated deformable mirror settings to estimate the field prior to evaluating the control shape. This paper outlines the algorithms used and presents our laboratory results.

Keywords: High-contrast imaging, coronagraphs, wavefront control, exoplanets, MEMS DMs

1. INTRODUCTION

The number of planets discovered orbiting other stars has soared over the past decade, exciting astronomers and the general public alike. While the science obtained has been extremely impactful, it has still been limited by the inability to directly image the companion planets. This is because the halo created from diffracted stellar light is many orders of magnitude brighter than the planet (for instance, an Earth-sized planet located 1 AU from its parent star is expected to be 10 billion times dimmer). Future plans for both large ground telescopes (e.g., Gemini, VLT, and Subaru) and forthcoming space observatories include provisions for techniques to create high-contrast, regions in the image close enough to the star where very dim companions can be seen with sufficient fidelity. A promising category of methods is known as *coronagraphy*. A coronagraph consists of a series of field stops and relay optics to suppress the starlight leakage due to diffraction into the planet detection area of the image. The first coronagraph was invented by Bernard Lyot to study the corona of the Sun.

Numerous new coronagraph designs for high-contrast have been proposed over the last decade with a number of them in advanced stages of technology development for potential use in a future space observatory or on large ground telescopes. These coronagraph designs are differentiated by various performance metrics, such as throughput, inner working angle (the closest angle to the star at which a planet can be observed), bandwidth, ease of implementation (a surrogate for cost), sensitivity, and robustness. Some are being considered for very high-contrast (greater than 10^{11}) and small inner working angles to enable imaging of terrestrial planets in the habitable zones of nearby stars. Unfortunately, however, all coronagraphs suffer from

Send correspondence to jkasdin@princeton.edu.

MEMS Adaptive Optics VI, edited by Scot S. Olivier, Thomas G. Bifano, Joel Kubby, Proc. of SPIE Vol. 8253, 825303 · © 2012 SPIE · CCC code: 0277-786X/12/$18 · doi: 10.1117/12.910634

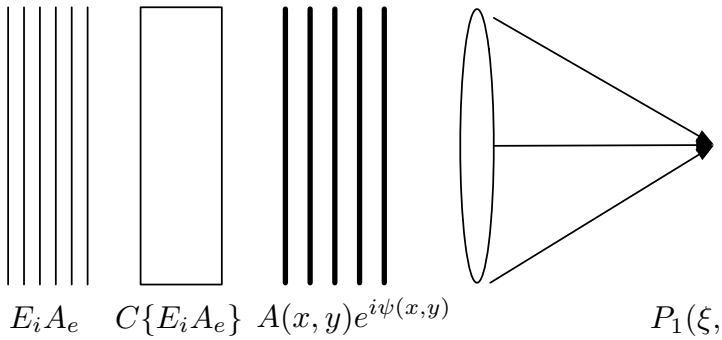

Figure 1. Propagation of a uniform input field E_i through an aperture of area A_e and a coronagraph represented by the linear operator $C\{E_i A_e\}$ to produce an amplitude and phase distribution $A(x,y)e^{i\psi(x,y)}$. $P_1(\xi,\eta)$ is the point spread function after passing through a focusing element.

the same limitation. Coronagraphic imaging is highly sensitive to aberrations created by small manufacturing errors on the optics, requiring wavefront control techniques to recover the regions of high contrast.

Like adaptive optics systems currently employed on most large telescopes, all proposed coronagraphic systems employ deformable mirrors to modify the phase of the wavefront, thus correcting the aberrations before creating an image. However, unlike traditional AO, the extreme sensitivity and desire for very high contrast requires correcting both the amplitude and phase of the aberrated wavefront using only measurements from the science camera (to eliminate non-common path error in the sensing path). It has been shown that using two-deformable mirrors in series can correct both amplitude and phase over a reasonably broad band of wavelengths.[1,2] In this paper we present the basic principals underlying how all coronagraphs achieve high contrast and then specifically describe the shaped pupil coronagraph being studied in the High Contrast Imagine Laboratory (HCIL) at Princeton. We then describe the techniques and algorithms we have developed for estimating and correcting both the amplitude and phase of the wavefront using two Boston Micromachines MEMS deformable mirrors acting in series. Finally, we present our recent laboratory results creating dark holes over a 10% band of wavelengths on both sides of the stellar image.

2. CORONAGRAPHS ARE AMPLITUDE DEVICES

All coronagraphs are based on the same fundamental principal: changing the amplitude of the electric field at some exit pupil prior to the final focusing element. While they may differ in the specifics, which can change the overall performance metrics, all must modify amplitude. We summarize here a general treatment for finding the contrast achievable by any coronagraph.[3]

Figure 1 is a schematic of the optical train of any coronagraph. It consists of a uniform, on-axis entrance field (the light from the star) of magnitude E_i entering an aperture with shape and transmission given by $A_e(x,y)$. The composite field, $E_i A_e(x,y)$, is passed through a coronagraph that we treat as a linear operator, $\mathcal{C}\{\cdot\}$, that changes the amplitude and phase of the field such that at the exit of the coronagraph the field is

$$E_1(x,y) = \mathcal{C}\{E_i A_e(x,y)\} = A(x,y)e^{i\psi(x,y)} \tag{1}$$

where $A(x,y)$ is the modified amplitude distribution due to the coronagraph and $\psi(x,y)$ is the phase change. We assume a perfect imaging element so that the final point spread function is just the properly normalized square of the Fourier transform of the exit field $E_1(x,y)$.

In the absence of a coronagraph, the nominal point spread function of the telescope is just the square of the Fourier transform of the entrance field times the aperture,

$$P_0(\xi,\eta) = |F(\xi,\eta)|^2 = \left|\hat{A}_e\left(\frac{\xi D}{\lambda f}, \frac{\eta D}{\lambda f}\right)\right|^2 \tag{2}$$

where D is the telescope diameter, f is the focal length, and $F(\xi,\eta) = \hat{A}_e = \mathcal{F}\{A_e(x,y)\}$ is the Fourier transform of $A_e(x,y)$. Note that we have normalized the input field to have unit amplitude. For a circular entrance aperture, this point spread function is the well known Airy function. Unfortunately, the Airy rings in the wings of the PSF where a planet is found are many orders of magnitude brighter than the planet.

With a coronagraph in place, the new point spread function becomes

$$P_1(\xi,\eta) = \left|\mathcal{F}\{A(x,y)e^{i\psi(x,y)}\}\right|^2. \tag{3}$$

The purpose of the coronagraph is to create a region (or regions) of high contrast in the image plane; these are often called the *discovery space* or *dark hole* of the coronagraph. We represent this region by $\Delta\Omega$. It is bounded by the *inner* and *outer working angles* of the coronagraph. We introduce a contrast metric, C, defined as the ratio of the integrated intensity in the discovery space to the peak of the point spread function of the open aperture system,

$$C = \frac{\int_{\Delta\Omega} P_1(\xi,\eta)d\xi d\eta}{T_\Omega \Delta\Omega P_0(0)} \tag{4}$$

where we have also normalized by the throughput of the coronagraph system at the inner working angle, T_Ω. Since we are assuming that the system without the coronagraph is just an open aperture, $F(0,0) = \int\int A_e(x,y)dxdy = A$, the entrance area of the telescope. This let's us rewrite Eq. 4,

$$C = \frac{1}{T_\Omega \Delta\Omega A^2}\left[\int_{-\infty}^{\infty}\int_{-\infty}^{\infty} P_1(\xi,\eta)d\xi d\eta - \int\int_{\Delta C} P_1(\xi,\eta)d\xi d\eta\right] \tag{5}$$

where ΔC is the complimentary region of the image plane to the discovery space.

From Parseval's theorem,

$$\int_{-\infty}^{\infty}\int_{-\infty}^{\infty} |F(\xi,\eta)|^2 d\xi d\eta = \int\int |A(x,y)|^2 dxdy \tag{6}$$

where, again, $A(x,y)$ is the amplitude distribution in the exit pupil. This allows us to further rewrite the contrast as

$$C = \frac{\int\int |A(x,y)|^2 dxdy}{T_\Omega \Delta\Omega A^2}\left[1 - \frac{\int\int_{\Delta C} P_1(\xi,\eta)d\xi d\eta}{\int_{-\infty}^{\infty}\int_{-\infty}^{\infty} P_1(\xi,\eta)d\xi d\eta}\right]. \tag{7}$$

Eq. 7 is the most general expression for the contrast created from an on-axis field passing through *any* coronagraph. It shows that coronagraphs achieve contrast in one of two ways. The first is to reduce the field amplitude at the exit of the coronagraph, making the leading factor (the integral of $|A(x,y)|^2$ in Eq. 7) sufficiently small. Examples of such coronagraphs include the Lyot, Bandlimited Lyot, Vector Vortex, Four Quadrant Phase Mask, Achromatic-Intefero Coronagraph (AIC), and any other coronagraph that modifies an intermediate image to change the amplitude of the exit pupil field. In fact, a perfect bandlimited Lyot coronagraph makes $A(x,y)$ identically zero, thus removing all starlight ($C = 0$).

The second approach to creating contrast is to make the factor in brackets small. This is accomplished by making the ratio of integrated intensity outside the discovery space to the total integrated intensity as close to one as possible. In other words, by concentrating as much energy as possible outside the discovery space, high contrast can be achieved. All apodized coronagraphs operate this way, including smooth apodizers, shaped pupils, and pupil mapping coronagraphs. The Apodized Prolate Lyot Coronagraph (APLC) creates high-contrast through a combination of both terms. We note that for every imaging system, with or without a coronagraph, the discovery space $\Delta\Omega$ can be made sufficiently far away (large enough inner working angle) to achieve any desired contrast. However, to achieve contrast at a sufficiently small inner working angle in a reasonable size telescope, the amplitude of the field at the exit pupil must be changed. Slepian[4] showed, through the finite uncertainty principal,[5] that the optimal apodization that maximally concentrates light is the prolate spheroidal wave function.

Coronagraphs are effective to the extent that they successfully achieve the desired amplitude distribution at the exit pupil. Unfortunately, real systems have aberrations. For instance, if the input field has phase aberrations, the coronagraph will fail to achieve the desired amplitude or the apodization will fail to create the desired concentration. In ground AO, a deformable mirror is used to conjugate the aberrations and recreate the flat field in order to recover performance. Such field conjugation is effective up to the point where performance is dominated by uncorrected amplitude errors, which sets a limit to most ground high-contrast systems. In space systems, where extremely high contrast is desired to enable terrestrial planet finding in the habitable zone, the ability to correct both phase and amplitude is a requirement. Up to now, amplitude has been corrected by using the quadrature component of the phase off a single DM to create a dark hole on only one side of the image plane.[6] Correcting both amplitude and phase for a symmetric dark hole requires two deformable mirrors, either in a Michelson configuration[1] or in series.[7] In the remainder of this paper we describe our configuration and algorithms for using two DMs in series to correct amplitude and phase with a Shaped Pupil coronagraph.

3. THE SHAPED PUPIL CORONAGRAPH

Shaped pupils produce apodizations using only binary masks that either block or allow transmission across the pupil. We design shaped pupils by maximizing the throughput subject to constraints on the contrast and dark hole size and shape in the image plane. Because the effect of the shaped pupil on the amplitude distribution in the image plane can be written as a linear operator, optimal solutions can be found very efficiently. All of our past designs for shaped pupils, however, have been done for one-dimensional geometries;[8,9] the solution is then continued to 2 dimensions using symmetry. Examples include barcode masks, checkerboard masks and concentric ring masks. Recently we developed a new technique that allows us to directly optimize the most general shaped pupil possible in two dimensions.[10,11]

The result is a shaped pupil with the maximum possible throughput and smallest inner working angle. It also allows us to design shaped pupils for arbitrary geometries, opening the possibility of use with on-axis telescopes incorporating central obstructions and spiders. We have also been able to design shaped pupils for segmented telescopes. We use this to design new shaped pupil masks consistent with a coronagraph associated to a wavefront control system. Knowing that the shaped pupil will be followed by a wavefront controller, we design only for limited contrast and for a dark hole shape consistent with the wavefront control. In particular, we design masks to achieve contrasts of only 10^{-5} or 10^{-6} with the wavefront control system accomplishing the rest.

Figure 2 shows new shaped pupils designed for three on-axis monolithic telescopes: the Subaru telescope, the Gemini south telescope and the upcoming SPICA space telescope. Inner working angles of 3 λ/D and smaller are achieved for contrast ranging from 10^{-6} to 10^{-7}. The diffraction spikes due to the spiders have been eliminated in the high contrast region. Finally, Figure 3 shows two shaped pupil masks designed for the segmented mirrors of the Keck telescope and the James Webb Space Telescope (JWST). At a contrast of 10^{-5} the performance of the second mask is comparable to currently planned coronagraphs on the observatory, but with a smaller inner working angle of 5 λ/D and a throughput of 45%.

The final step in the design process is to combine the new shaped pupil designs with the stroke minimization controller to achieve the deeper 10^{-10} dark holes. We are in the process of manufacturing new shaped pupils to put in the laboratory and combine with the wavefront control system.

4. MONOCHROMATIC CORRECTION OF AMPLITUDE AND PHASE

Using a Taylor series expansion of the aberrated electric field it has been shown that, to first order, two DMs in series are capable of correcting both amplitude and phase aberrations, resulting in symmetric dark holes in the image plane.[6] Physically, such a controller relies on the amplitude-to-phase mixing resulting from propagation of the field between non-conjugate planes (the first DM to the second). If the magnitude of the first DM's actuation is chosen correctly, then it can exactly conjugate the amplitude variations at the pupil plane at which point the second DM, assumed to be at a conjugate pupil, can correct the residual phase

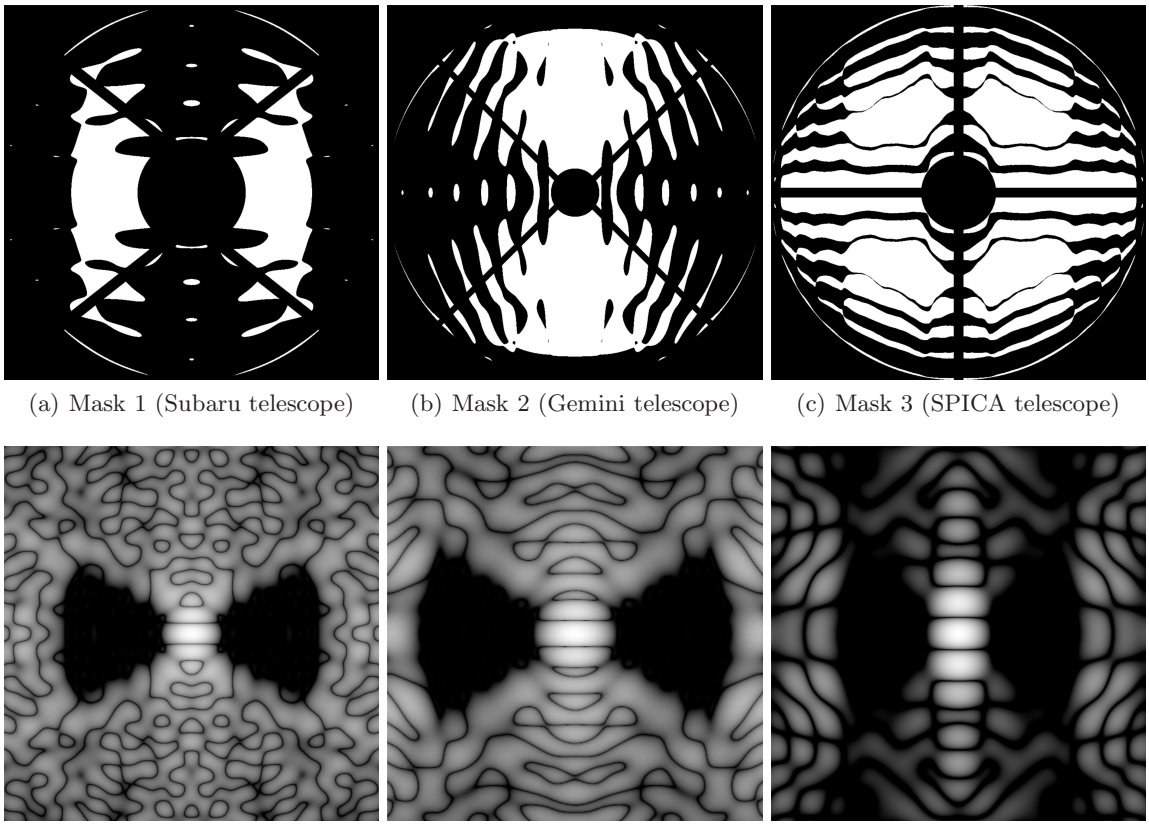

(a) Mask 1 (Subaru telescope) (b) Mask 2 (Gemini telescope) (c) Mask 3 (SPICA telescope)

(d) PSF of Mask 1 (e) PSF of Mask 2 (f) PSF of Mask 3

Figure 2. Top: masks designed, from left to right, for the Subaru telescope, the Gemini south telescope, and the SPICA telescope. Bottom: corresponding point-spread functions. The IWA are 2.3, 3 and 3.3 λ/D. The outer working angles are 8 and 12 λ/D. Contrast is 10^{-6} in the first and third cases and 10^{-7} in the second case.

aberrations. Algorithmically this is achieved through a number of methods, each with its set of advantages and disadvantages. In general focal plane wavefront sensing methods are broken down into a wavefront estimation step followed by a control step where the correction is decided.

4.1 Stroke Minimization in Monochromatic Light

The stroke minimization algorithm uses the estimate of the image plane electric field to correct the wavefront by minimizing the actuator stroke subject to a target contrast value.[6] Expressing the DM actuator amplitudes as a vector, X, the optimization problem can be written as

$$\begin{array}{ll} \text{minimize} & \sum_{k=1}^{N} a_k^2 = XX^T \\ \text{subject to} & I_{DZ} \leq 10^{-C}. \end{array} \tag{8}$$

where a_k is the commanded height of actuator k, I_{DZ} is the residual intensity in the dark hole after correction, and C is the target contrast. We solve the optimization by approximating I_{DZ} as a quadratic form,

$$I_{DZ} \cong \left(\frac{2\pi}{\lambda}\right)^2 XMX^T + \frac{4\pi}{\lambda} X\Im\{b^T\} + d \tag{9}$$

where b is a vector describing the interaction between the DM shape and the aberrated field, d is a vector that expresses contrast in the dark hole, and M is the matrix which describes the linearized mapping of DM

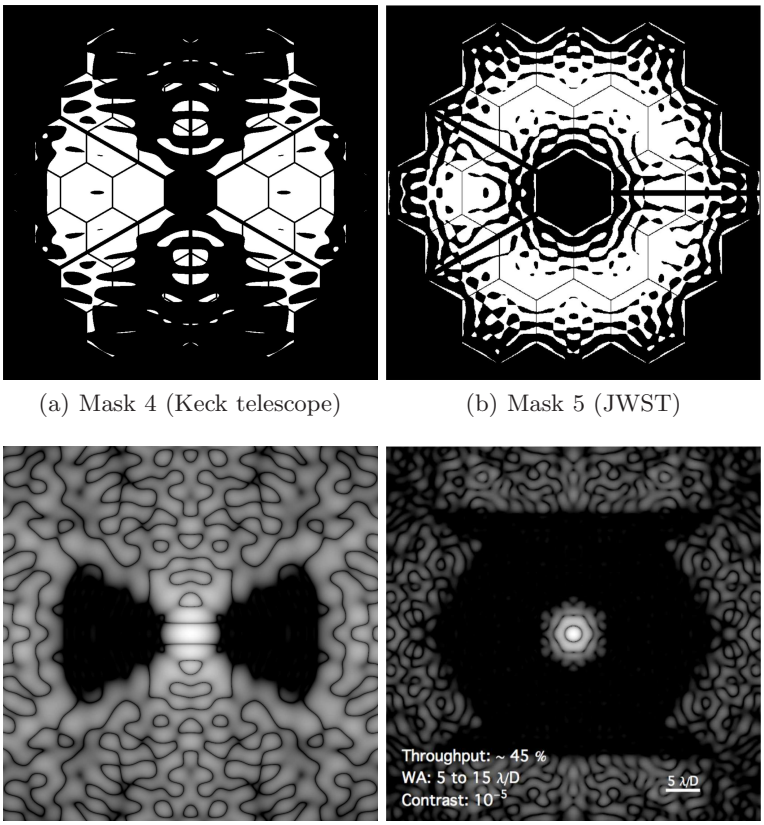

(a) Mask 4 (Keck telescope) (b) Mask 5 (JWST)

(c) PSF of Mask 4 (d) PSF of Mask 5

Figure 3. Top: masks designed for the Keck telescope (left), and the JWST (right). Bottom: corresponding point-spread functions. The IWA are 3 and 5 λ/D. The outer working angles are 14 and 15 λ/D. Contrast is 10^{-7} in the first case and 10^{-5} in the second case.

actuation to intensity in the dark hole. The resulting quadratic subprogram is easily solved by augmenting the cost function via Lagrange multiplier, μ, and solving for the commanded actuator heights:

$$J = X\left(\mathcal{I} + \mu\left(\frac{2\pi}{\lambda}\right)^2 M\right)X^T + \mu\frac{4\pi}{\lambda}X\Im(b^T) + \mu(d - 10^{-C}) \tag{10}$$

$$X_{opt} = -\mu\Im(b)\left(\frac{\lambda}{2\pi}\mathcal{I} + \mu\frac{2\pi}{\lambda}M\right)^{-1}. \tag{11}$$

We find the optimal actuator commands via a line search on μ to minimize the augmented cost function (Eq. (10)).

It is shown in Pueyo et al.[6] that since this is a quadratic subprogram of the full nonlinear problem we can iterate to reach any target contrast. In addition to regularizing the problem of minimizing the contrast in the search area, minimizing the stroke has the added advantage of keeping the actuation small and thus within the linear approximation. In the experiment, the second MEMS deformable mirror is not conjugate to the pupil plane in an effort to minimize the number of optics in the system. However, this does not change the fact that two DMs in series can correct both amplitude and phase aberrations at the pupil plane. Both MEMS deformable mirrors use amplitude-to-phase mixing from their individual Fresnel propagations to suppress the aberrations in the pupil plane. Since there is no constraint in the control algorithm that

the second deformable mirror only conjugate phase aberrations, the problem isn't restricted to only the first deformable mirror correcting amplitude aberrations.

If the DM model and its transformation to the electric field (embedded in the M matrix) were perfectly known, the achievable monochromatic contrast using stroke minimization is limited only by estimation error as long as the DM actuation remains within the bounds of the linearization. MEMS DMs allow us to create very accurate models with little computational cost because they provide relatively linear response at extremely low stroke and do not exhibit hysteresis.

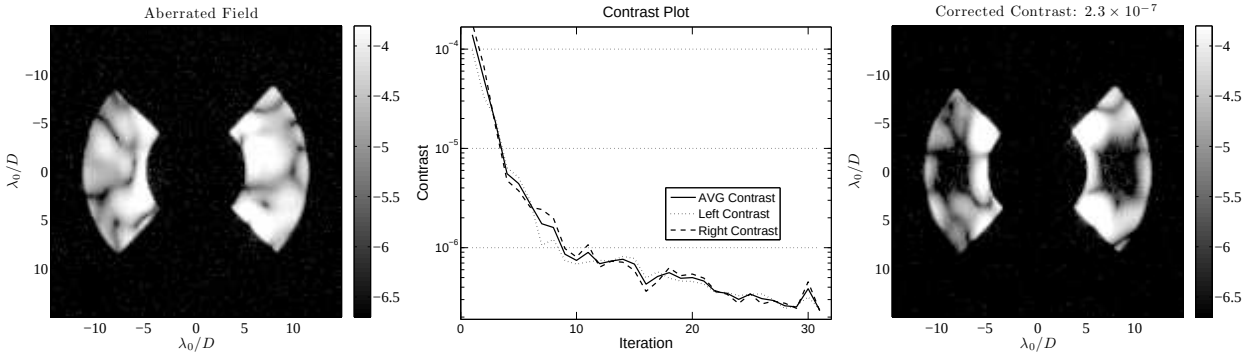

(a) Initial Aberrations (b) Contrast vs. Iteration (c) Corrected Image

Figure 4. Experimental results of sequential MEMS DM correction using the discrete time extended Kalman filter with 2 image pairs to build the image plane measurement, z_k. The dark hole is a square opening from 7–10 x -2–2 λ/D on both sides of the image plane. Final contrast is 2.3×10^{-7} on both sides of the image plane. Image units are log(contrast).

Fig. 4 shows current laboratory results using Stroke Minimization with a Kalman filter estimator.[12] The contrast after 30 iterations of the correction algorithm reached 2.3×10^{-7} on both sides of the image plane in monochromatic light, achieving nearly three orders of magnitude additional contrast from the initial value of 1.3934×10^{-4}.

5. BROADBAND WAVEFRONT CONTROL USING STROKE MINIMIZATION

Narrowband correction schemes ($\Delta\lambda/\lambda \leq 2\%$) for high contrast imaging have been well demonstrated.[13] Nevertheless, achieving broadband correction is key to raising the TRL level of wavefront control algorithms. Generating a null for each wavelength separately to spectrally characterize a target would be prohibitively slow because of the large number of exposures required to estimate the electric field. A broadband algorithm reduces the number of exposures, and hence the time required to spectrally characterize a target. Increasing the bandwidth is also the easiest way to increase the number of photons in an inherently photon limited system, reducing the exposure time required to achieve a planetary detection. Thus, broadening the spectral range of the wavefront correction will improve the overall efficiency of a planet finding mission and will allow for fewer parallel beam paths, making it cheaper and less complex to measure over a broad bandwidth. It has been shown that two DMs in series can be used to correct over a broader range of wavelengths by incorporating wavelength expansions of the aberrated electric field propagation.[1] This was proven by expressing the aberrated field at a pupil, given in terms of the amplitude and phase aberrations, $r(x, y)$ and $\phi(x, y)$ respectively, as a Fourier series,

$$E_{pup}(u, v, \lambda) = A(u, v)\Sigma_{m,n}\Sigma_k \; i^k \; \frac{f_{m,n}^{-k}\lambda_0^k}{\lambda^k} \; e^{i\frac{2\pi}{D}(mu+nv)}. \tag{12}$$

We created a broadband control algorithm by augmenting the cost function in the stroke minimization algorithm with multiple wavelengths. Providing estimates for this algorithm becomes more complicated

because it requires field values at multiple wavelengths. Taking estimates for each wavelength is no better than correcting each wavelength individually because estimation is the most costly component of the control algorithm and the time required is limited by exposure time, not computation. We solved this by extrapolating a single monochromatic estimate using the DM Diversity algorithm to higher and lower wavelengths by approximating the pupil field of Eq. 12. Assuming that the amplitude distributions at the pupil are wavelength independent, only the zeroth order term, $k = 0$, is non-zero. Assuming the phase distributions scale inversely proportional to wavelength we rewrite the phase with the relationship $\Sigma_{m,n}(mu + nv)/D = \phi(u,v)/\lambda = \lambda_0/\lambda\ \phi_0(u,v)$ to approximate the pupil plane electric field as

$$E_{pup}(u,v,\lambda) \approx A(u,v)e^{i2\pi\frac{\lambda_0}{\lambda}\phi_0(u,v)}. \tag{13}$$

Assuming a linear, wavelength dependent, transformation between the pupil and image plane $\mathcal{C}_\lambda$ (e.g. the optical Fourier transform) we can use Eq. 13 to describe the electric field estimate at an arbitrary wavlength λ as a function of the image plane electric field estimate taken at the original wavelength λ_0 using the DM-diversity algorithm. With the wavelength dependence only appearing in the phase of the pupil field and in the pupil to image transformation the electric field estimate at a new wavelength becomes

$$E_{est}(x,y,\lambda) = \mathcal{C}_\lambda \left\{ \frac{\mathcal{C}_{\lambda_0}^{-1}\{E_{est}(\lambda_0)\}^{\frac{\lambda_0}{\lambda}}}{\left|\mathcal{C}_{\lambda_0}^{-1}\{E_{est}(\lambda_0)\}\right|^{\frac{\lambda_0}{\lambda}-1}} \right\}. \tag{14}$$

With the extrapolation technique provided by Eq. 14 in place, the simplest approach to augmenting the stroke minimization algorithm, Eq. 10, is to demand a contrast constraint at a wavelength above and below the central wavelength. The optimization is then written as

$$\begin{aligned}
\text{minimize} \qquad & \sum_{k=1}^{N} a_k^2 = XX^T \\
\text{subject to:} \qquad & I_{DZ}(\lambda_0) \le 10^{-C_{\lambda_0}}, \\
& I_{DZ}(\lambda_1) \le 10^{-C_{\lambda_1}}, \\
& I_{DZ}(\lambda_2) \le 10^{-C_{\lambda_2}} \\
\text{where} \qquad & \lambda_1 = \gamma_1\lambda_0 \\
& \lambda_2 = \gamma_2\lambda_0\ ,
\end{aligned} \tag{15}$$

which minimizes actuator strokes, X, under the constraint that a particular contrast, C_i, be achieved in three separate wavelengths, λ_i. The cost function then takes on the same basic form, but now includes multiple wavelengths:

$$\begin{aligned}
J =& X\left[\mathcal{I} + \mu\frac{4\pi^2}{\lambda_0^2}\left(M_{\lambda_0} + \delta_1 M_{\lambda_1} + \delta_2 M_{\lambda_2}\right)\right]X^T + \mu\frac{4\pi}{\lambda_0}\left[\Im\{b_{\lambda_0}\} + \delta_1\Im\{b_{\lambda_1}\} + \delta_2\Im\{b_{\lambda_2}\}\right]X^T \\
& + \mu\left[\left(d_{\lambda_0} - 10^{-C_{\lambda_0}}\right) + \delta_1\left(d_{\lambda_1} - 10^{-C_{\lambda_1}}\right) + \delta_2\left(d_{\lambda_2} - 10^{-C_{\lambda_2}}\right)\right].
\end{aligned}$$

where M_λ describe the effect on the image plane intensity from the DM actuation, b_λ is intensity from the interaction of the DMs with the aberrated field, and d_λ is intensity of the uncorrected aberrated field. The multipliers δ_1 and δ_2 allow us to parameterize a single Lagrange multiplier in the cost function. In the more general case with three Lagrange multipliers it is possible that the global minimum of the function would not result in constant contrast at each wavelength. This approach to stroke minimization, what we call "windowed stroke minimization", makes the optimization in wavelength tractable and allows for estimation

only at a single wavelength, which reduces the number of exposures required for correction over a bandwidth defined by the upper and lower bounding wavelengths.

Fig. 5 shows laboratory results at the HCIL creating symmetric dark holes in broadband using the windowed stroke minimization algorithm and extrapolated estimation from Eq. 14. Starting from an initial contrast of 1.0183×10^{-4} (Fig. 5(a)) the current achievable contrast by extrapolating estimates is 5.47×10^{-6} over approximately a 10% band (Fig. 5)). Fig. 5(b) shows the achieved contrast as a function of wavelength.These results represent the only algorithm to date which has proven symmetric dark holes in broadband light by simultaneously correcting amplitude and phase aberrations at multiple wavelengths. Comparing to the monochromatic case the algorithm is achieving a contrast level more than an order of magnitude worse, but the bandwidth of this suppression level is much higher.

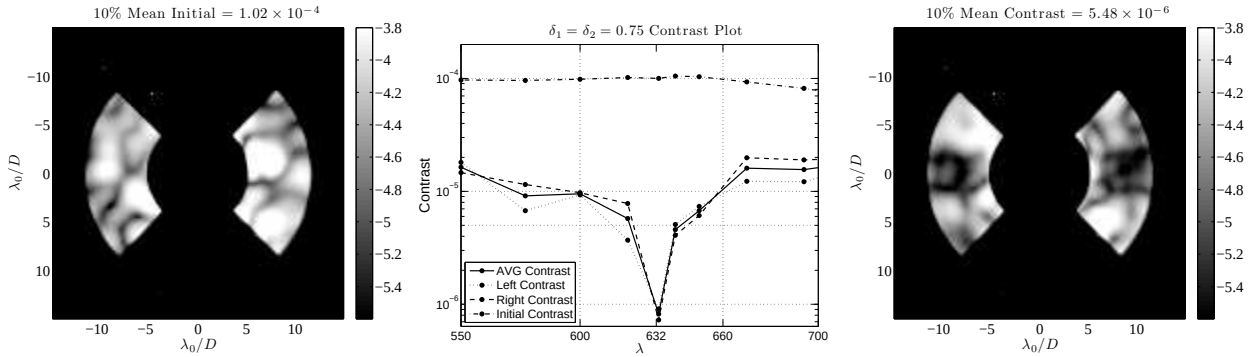

(a) Initial Aberrations, 10% (b) Final Contrast vs. Wavelength (c) Final Image, 10%

Figure 5. Extrapolating a single estimate to the bounding wavelengths to suppress the field in a 10% band using MEMS DMs. Final contrast is 5.47×10^{-6} averaged over the filters in a 10% band.

Acknowledgements

This work was partially performed under NASA contract NNX09AB96G.

REFERENCES

1. L. Pueyo and N. J. Kasdin, "Polychromatic Compensation of Propagated Aberrations for High-Contrast Imaging," *ApJ* **666**, pp. 609–625, Sept. 2007.
2. S. Shaklan, J. Green, and D. Palacios, "The terrestrial planet finder coronagraph optical surface requirements," *Proceedings of SPIE* **6265**, pp. pp. 62651I–1 – 62651I–12, 2006.
3. N. J. Kasdin, A. Carlotti, L. Pueyo, T. Groff, and R. Vanderbei, "Unified coronagraph and wavefront control design," in *Proceedings of the SPIE Optics and Photonics Conference*, **8151**(33), 2011.
4. D. Slepian, "Analytic solution of two apodization problems," *Journal of the Optical Society of America* **55**(9), pp. 1110–1115, 1965.
5. H. J. Landau and H. O. Pollack, "Prolate spheroidal wave functions, fourier analysis and uncertainty—ii," *The Bell System Technical Journal* , pp. 65–84, January 1961.
6. L. Pueyo, J. Kay, N. Kasdin, T. Groff, M. McElwain, A. Give'on, and R. Belikov, "Optimal dark hole generation via two deformable mirrors with stroke minimization," *Applied Optics* **48**(32), pp. 6296–6312, 2009.
7. S. B. Shaklan and J. J. Green, "Reflectivity and optical surface height requirements in a broadband coronagraph. 1.Contrast floor due to controllable spatial frequencies," *Applied Optics* **45**, pp. 5143–5153, July 2006.
8. D. Spergel and J. Kasdin, "A Shaped Pupil Coronagraph: A Simpler Path towards TPF," in *American Astronomical Society Meeting Abstracts*, *Bulletin of the American Astronomical Society* **33**, p. 1431, Dec. 2001.

9. R. J. Vanderbei, D. N. Spergel, and N. J. Kasdin, "Spiderweb Masks for High-Contrast Imaging," *The Astrophysical Journal* **590**, pp. 593–603, June 2003.
10. A. Carlotti, R. Vanderbei, and N. J. Kasdin, "Optimal pupil apodizations of arbitrary apertures for high-contrast imaging," *Opt. Express* **19**, pp. 26796–26809, Dec 2011.
11. R. J. Vanderbei, "Fast Fourier optimization: sparsity matters," *Mathematical Programming Computation* **590**, Jan. 2012.
12. T. Groff and N. Kasdin, "Designing an optimal estimator for more efficient wavefront correction," in *Proceedings of SPIE*, **8151**, p. 81510X, 2011.
13. J. Trauger and W. Traub, "A laboratory demonstration of the capability to image an earth-like extrasolar planet," *Nature* **446**(7137), pp. 771–773, 2007.